Selective Vapor Phase Doping of Pt Nanoparticles into Phase-Controlled Nanoalloys

-- Supporting Information --

Nithin Poonkottil[†], Ranjith K. Ramachandran[†], Eduardo Solano[∇], Nadadur Veeraraghavan Srinath[‡], Ji-Yu Feng[†], Andreas Werbrouck[†], Michiel Van Daele[†], Matthias Filez[†], Matthias M. Minjauw[†], Hilde Poelman[‡], Alessandro Coati[⊥], Christophe Detavernier[†] and Jolien Dendooven*[†]

† Conformal Coating of Nanostructures (CoCooN), Department of Solid State Sciences, Ghent University, Krijgslaan 281 (S1), 9000 Ghent, Belgium

‡ Laboratory for Chemical Technology, Ghent University, Technologiepark 125, B-9052 Zwijnaarde, Ghent, Belgium

⊥ *Synchrotron SOLEIL, SixS Beamline, L'Orme des Merisiers, Saint-Aubin, BP48, 91192 Gif-sur-Yvette, France*

∇ *ALBA Synchrotron Light Source, NCD-SWEET beamline, Carrer de la Llum, 2-26, 08290, Cerdanyola del Vallès, Spain*

E-mail: Jolien.Dendooven@Ugent.be

Composition determination

To determine the equivalent thickness of the Pt nanoparticle samples and calculate the composition of the Pt-Sn bimetallic nanoparticles, a calibrated X-ray fluorescence (XRF) method was employed as reported before[1]. For the construction of the XRF calibration curves, a series of pure ALD Pt and SnO_2 films with different thicknesses were deposited on a silicon substrate with native oxide. After the deposition, the thickness of each film was measured using X-ray reflectivity (XRR). From the thickness, the specific weight of Pt and SnO_2 was calculated assuming the densities of the films equal to bulk Pt and SnO_2. On each sample, an XRF measurement was done using an integration time of 100s. The XRF intensity counts (i.e., integration of the Pt Lα or Sn Lα fluorescence signal) and specific weight of Pt and Sn were plotted against the thickness of the films as measured by XRR. This in turn yields a calibration curve which could be used to determine the equivalent thickness of Pt nanoparticles and the composition of the synthesized Pt-Sn nanoparticles (Figure S1)

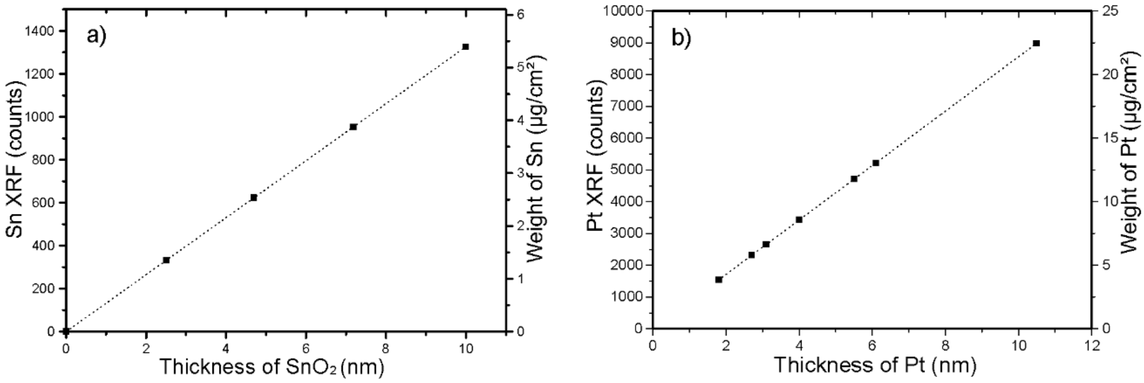

Figure S1. Variation of Sn (a) and Pt (b) Lα XRF counts (left y-axis) and weight (right y-axis) against the Pt and SnO_2 film thickness.

Composition as a function of temperature

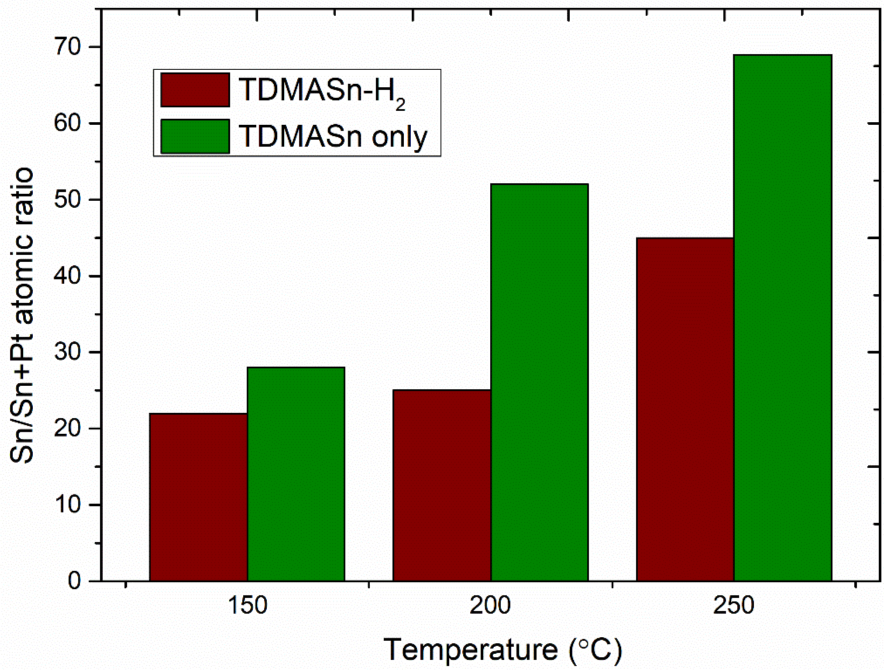

Figure S2: Sn/Sn+Pt atomic ratio for the TDMASn only and TDMASn-H_2 process. The TDMASn only process led to higher Sn/Sn+Pt atomic ratio compared to the TDMASn-H_2 process, irrespective of the substrate temperature as stated in the main text.

In situ GISAXS patterns during TDMASn-H_2 process

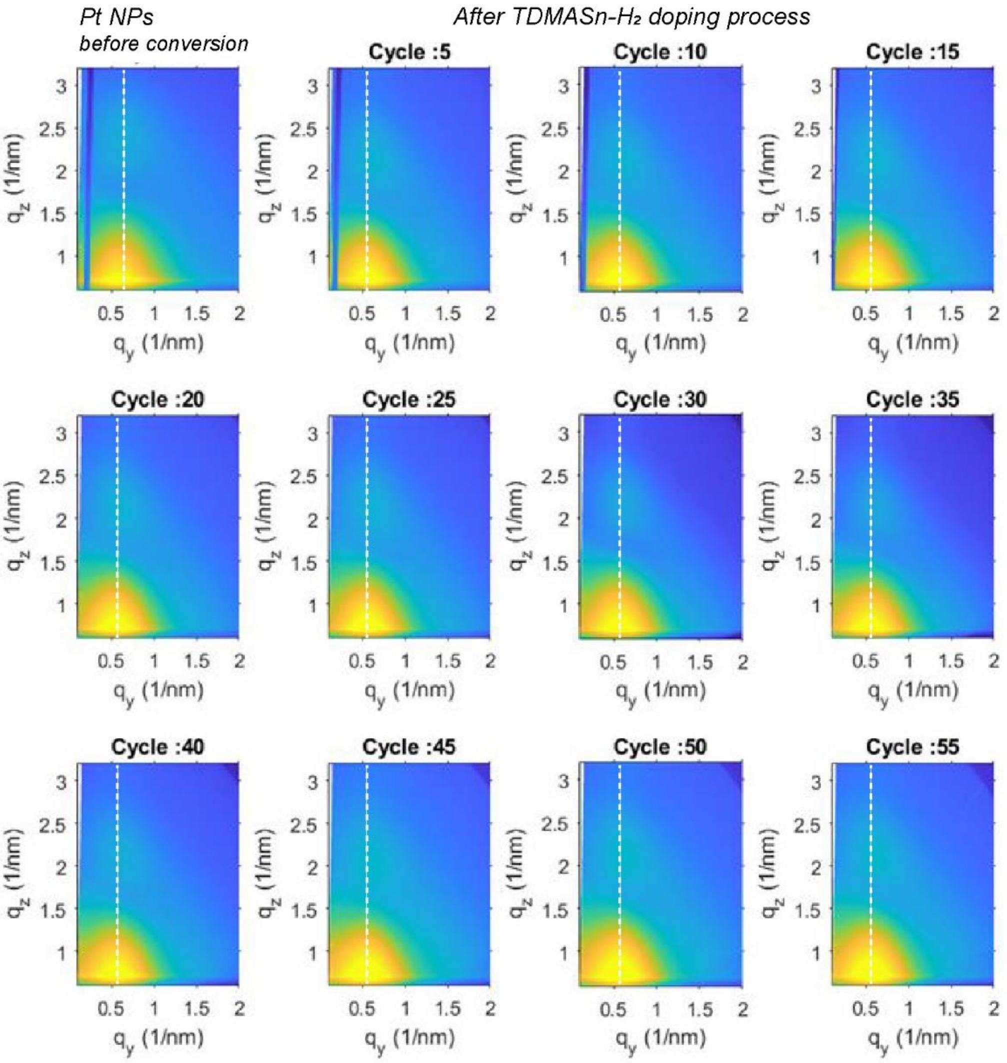

Figure S3. *In situ* GISAXS data during the TDMASn-H_2 process at 200 °C on ALD prepared Pt NPs (equivalent thickness of 3 nm). The first image shows the GISAXS pattern of the Pt NPs before doping and the rest shows the GISAXS images recorded after the TDMASn-H_2 doping cycles (the dashed vertical lines indicate the $q_{y,max}$ position). The images prove that a stable morphology is achieved after 5 doping cycles, in support of **Figure 4** in the main manuscript.

GISAXS data analysis

In order to extract the real space parameters such as the nanoparticle shape, size, and areal density from the q-space scattering data, we adopted an analysis approach, based on a geometrical model.[2] IsGISAXS[3] software was used to calculate the simulated 2D GISAXS patterns, using the extracted morphological parameters as input for the simulation. Then the measured data was compared to the simulated data to validate the proposed strategy. The best agreement between simulation and data was obtained when two particle shapes, full spheroids and hemispheroids are taken in a 1:1 ratio, where both particle geometries were described by the same particle height and radius. The particle radius was described by a lognormal distribution function, and a geometrical standard deviation s, was used to describe the distribution width. Assuming a Gaussian distribution for the particle aspect ratio (height/radius), a joint distribution for the particle height was implemented in IsGISAXS. The distribution width was then described by 0.05 times the central particle aspect ratio value. The distorted wave Born approximation (DWBA) was used to calculate the form factor, the perturbations caused by densely packed particles on a surface was described by the model of the graded interface.[4] The local monodisperse approximation (LMA) formalism, which is commonly used for polydispersed systems, was also used for the calculations,. The structure factor was calculated using a 1D paracrystal model, which is a regular 1D lattice with loss of long-range order. The distribution of the center-to-center distance D, was described by a Gaussian function with disorder parameter ω, calculated as $\omega = 0.4$ D.[2]

GISAXS simulations

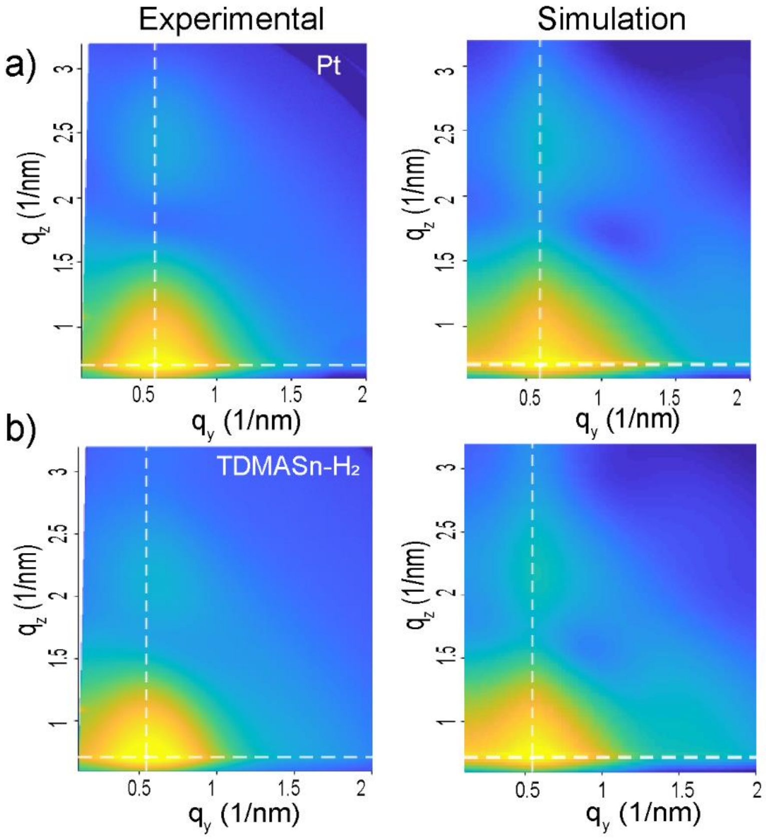

Figure S4. a) and b) Experimental (left) and simulated (right) GISAXS patterns of Pt nanoparticles (equivalent thickness of 3 nm) and after TDMASn-H_2 treatment, respectively (the dashed vertical lines indicate the $q_{y,max}$ position). Note that the experimental GISAXS patterns shown here are the same as those shown in **Figure 4** in the main text. The table indicates the parameters derived from the GISAXS simulation results. The given errors are based on our previous work[5] where an average error of 15% was derived for the GISAXS analysis of the particle center-to-center distance and width, and an error of 7% on the particle height of Pt nanoparticles grown with the $MeCpPtMe_3/O_2$ process.

Table S1. Morphological parameters obtained after the GISAXS simulations.

	Interparticle distance (nm)	Height (nm)	Width (nm)
Pt NPs	8.5 ± 1.3	4.5 ± 0.3	5.0 ± 0.8
After TDMASn-H_2	8.9 ± 1.3	5.0 ± 0.4	6.2 ± 0.9

Doping of WI Pt - Proof of concept

Table S2. BET surface area of wet impregnated (WI) Pt NPs

Sample	BET (m^2/g)	Average pore diameter (Å)	Pore volume (cm^3/g)
SiO_2	464.3 ± 5.2	61.0 ± 0.67	0.71 ± 0.01
Pt/SiO_2	375.7 ± 1.2	65.5 ± 0.60	0.62 ± 0.0022

The results are as expected with the BET surface area being lower for the impregnated Pt samples as the Pt is expected to block some pores and prevent N_2 adsorption. This is reflected in the total pore volume obtained whereby it is lower for the Pt impregnated sample.

The TDMASn-H_2 treatment was also performed on a WI Pt at substrate temperatures of 200 °C and 250 °C TEM/EDX images of these samples were taken after a redox treatment up to 600 °C. From the EDX mapping (Figure S5f and S6f), it is quite clear that there is less Sn than Pt on the NPs prepared at deposition temperature 200 °C compared to the one at 250 °C. This is in line with our strategy that the amount of Sn incorporated can be controlled by varying the substrate temperature. In other words, there is more Sn on the Pt NPs at 250 ° C deposition temperature compared to the one at 200 °C.

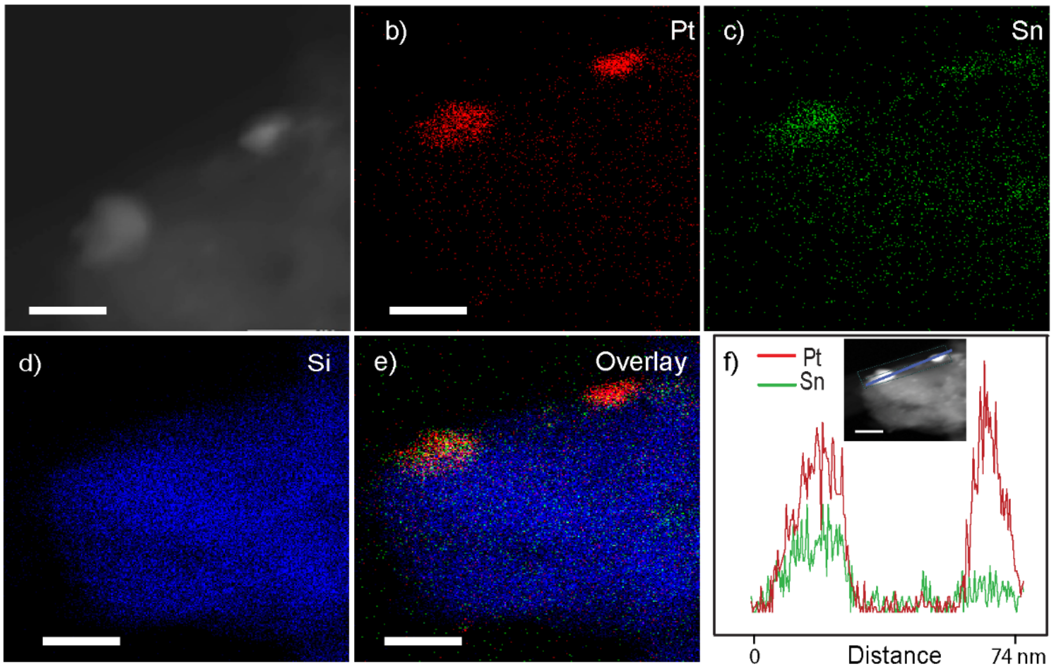

Figure S5: **a)** STEM image after the TDMASn-H_2 treatment at 200°C substrate temperature, followed by a redox treatment at 600°C. EDX mapping **b)** Pt **c)** Sn **d)** Si **e)** overlay (Pt+Sn+Si) **f)** EDX line scan, inset shows the region of the scan. All scale bars indicate 100 nm.

Figure S6 (relatively bigger NPs) and S7 (relatively smaller NPs) show that the doping of Sn on WI Pt/SiO2 occurs selectively on the Pt NPs in agreement with the other data presented in the main text of the manuscript.

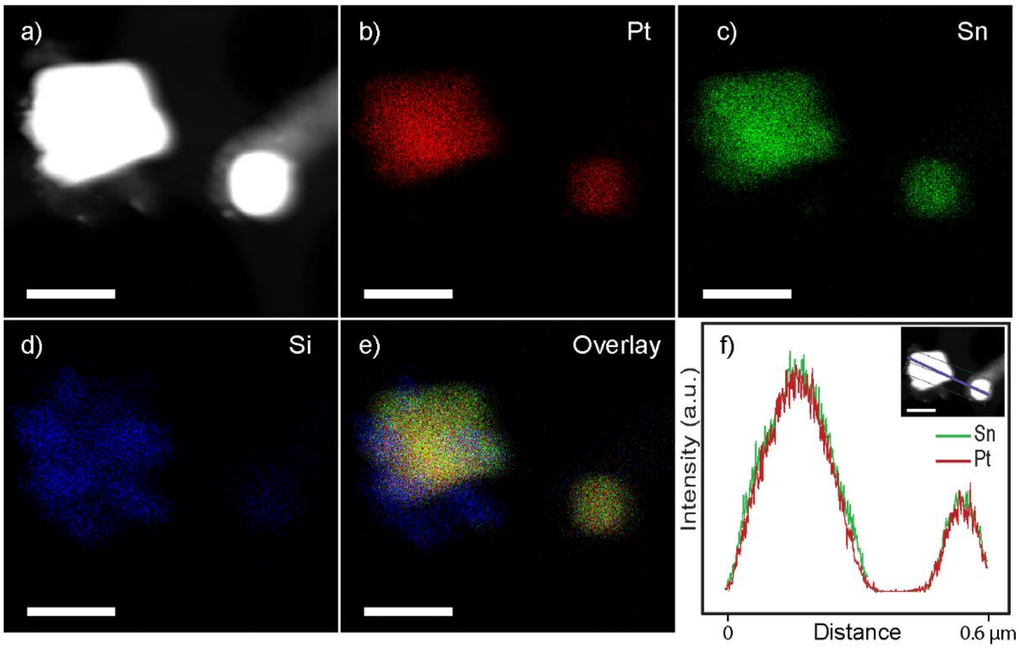

Figure S6. a) STEM image after the TDMASn-H_2 treatment on a WI Pt/SiO_2 (powder sample) at 250°C substrate temperature, followed by a redox treatment at 600°C. EDX mapping **b)** Pt **c)** Sn **d)** Si **e)** overlay (Pt+Sn+Si) **f)** EDX line scan, inset shows the region of the scan. All scale bars indicate 200 nm.

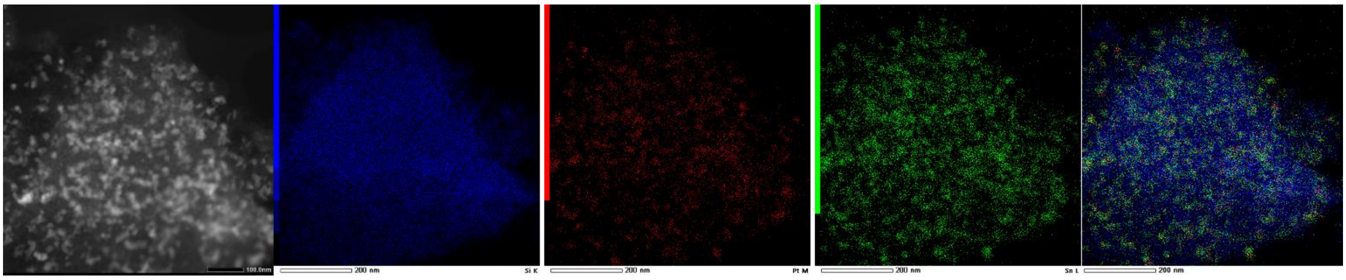

Figure S7: Additional STEM image (first) of the TDMASn-H2 treatment on WI Pt/SiO2 (powder sample at 250°C substrate temperature, followed by a redox treatment at 600°C. EDX mapping of Si, Pt, Sn and overlaid image are followed.

Preliminary data on the generality of the approach

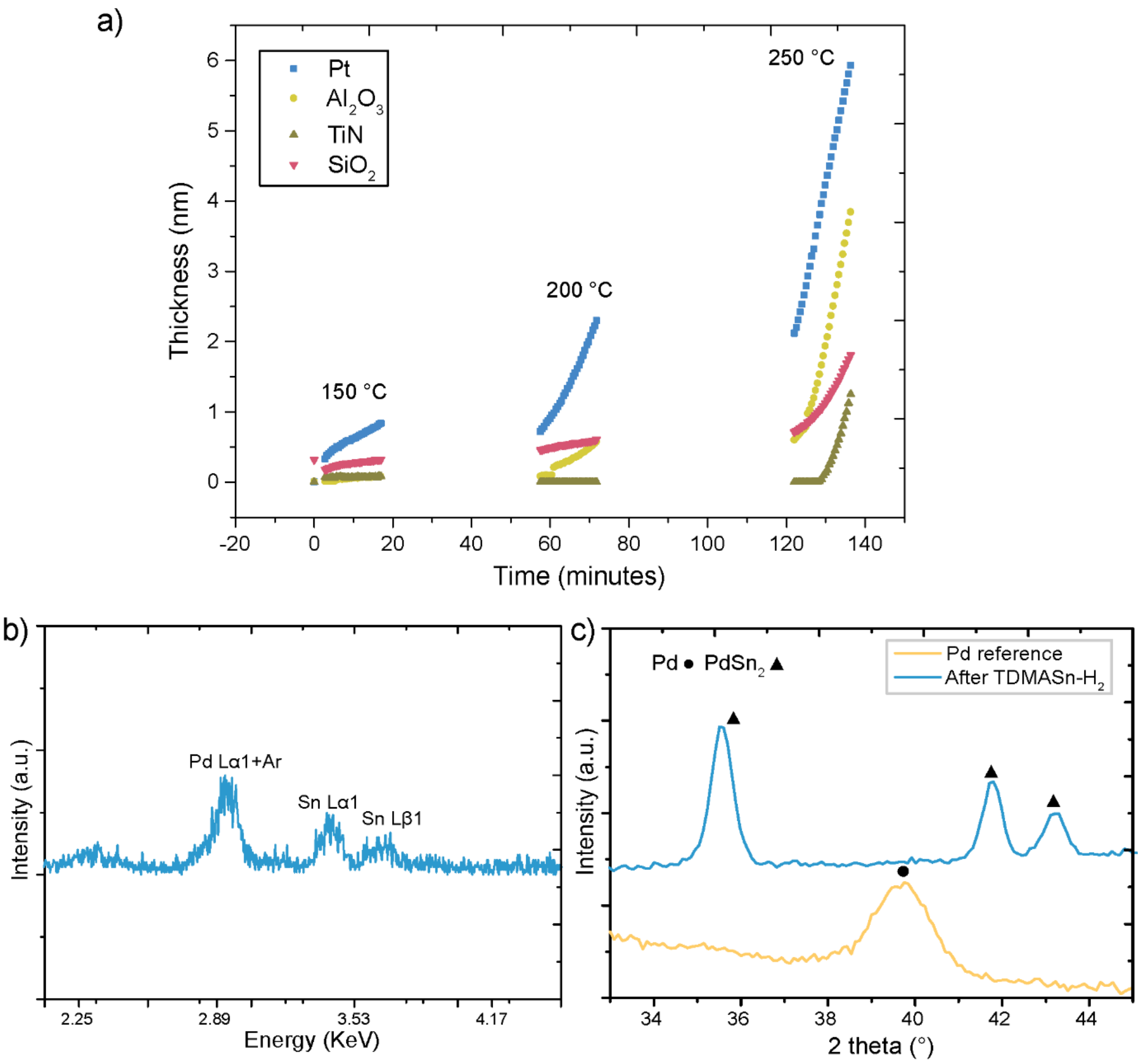

Figure S8: Generality of the selective decomposition and doping strategy. a) Decomposition experiments of TEMAV (a vanadium ALD precursor) on different substrates as obtained by in situ ellipsometry, b) XRF spectrum showing Pd and Sn peaks after the TDMASn-H2 process on Pd at a substrate temperature of 250°C and c) XRD spectra of Pd before and after the TDMASn-H2 treatment

References

1. Ramachandran, R. K.; Filez, M.; Dendooven, J.; Galvita, V. V.; Poelman, H.; Solano, E.; Fonda, E.; Marin, G. B.; Detavernier, C., Size-and Composition-Controlled Pt–Sn Bimetallic Nanoparticles Prepared by Atomic Layer Deposition. *RSC advances* **2017**, *7*, 20201-20205.

2. Dendooven, J.; Van Daele, M.; Solano, E.; Ramachandran, R. K.; Minjauw, M. M.; Resta, A.; Vlad, A.; Garreau, Y.; Coati, A.; Portale, G., Surface Mobility and Impact of Precursor Dosing During Atomic Layer Deposition of Platinum: In Situ Monitoring of Nucleation and Island Growth. *Physical Chemistry Chemical Physics* **2020**, *22*, 24917-24933.

3. Lazzari, R., Isgisaxs: A Program for Grazing-Incidence Small-Angle X-Ray Scattering Analysis of Supported Islands. *Journal of Applied Crystallography* **2002**, *35*, 406-421.

4. Lazzari, R.; Renaud, G.; Revenant, C.; Jupille, J.; Borensztein, Y., Adhesion of Growing Nanoparticles at a Glance: Surface Differential Reflectivity Spectroscopy and Grazing Incidence Small Angle X-Ray Scattering. *Physical Review B* **2009**, *79*, 125428.

5. Dendooven, J.; Ramachandran, R. K.; Solano, E.; Kurttepeli, M.; Geerts, L.; Heremans, G.; Rongé, J.; Minjauw, M. M.; Dobbelaere, T.; Devloo-Casier, K., Independent Tuning of Size and Coverage of Supported Pt Nanoparticles Using Atomic Layer Deposition. *Nature communications* **2017**, *8*, 1-12.